

ON THE DIFFERENT RADIO SOURCE POPULATIONS IN THE BUTCHER-OEMLER CLUSTERS ABELL 2125 AND 2645

K. S. DWARAKANATH

Raman Research Institute, C. V. Raman Avenue, Sadashivanagar, Bangalore 560 080, India

AND

F. N. OWEN

National Radio Astronomy Observatory, P.O. Box O, Socorro, NM 87801

Received 1999 February 25; accepted 1999 April 27

ABSTRACT

The Abell clusters 2125 and 2645 have different radio source populations, despite being very similar in richness (Abell class 4) and redshift (~ 0.25). The number density of radio sources in Abell 2125 is almost an order of magnitude more than that in Abell 2645, based on observations to the same optical and radio luminosities of the two clusters. About 30% of the radio sources in Abell 2125 shows signs of star formation, with the largest concentration of them in the southwest clump 2 Mpc from the cluster center. There is a bimodal distribution of Abell 2125 members in radio luminosity, with the majority below a spectral luminosity at 20 cm of $10^{23} \text{ W Hz}^{-1}$. This entire low-luminosity class of galaxies is absent in Abell 2645. Based on earlier observations, the blue galaxy fractions in Abell 2125 and Abell 2645 are known to be 0.19 and 0.03, respectively. Most of the blue galaxies responsible for the Butcher-Oemler effect in Abell 2125 were not detected in radio to a 20 cm luminosity limit of $1.4 \times 10^{22} \text{ W Hz}^{-1}$. The current supernova rate in these blue galaxies is unlikely to be more than a few times the current Galactic supernova rate. The different dynamical states of the two clusters might be responsible for the differences in the radio source populations observed in these two clusters, as well as the Butcher-Oemler effect.

Key words: galaxies: clusters: individual (Abell 2125, Abell 2645) — galaxies: starburst — radio continuum

1. INTRODUCTION

The Butcher-Oemler (B-O) effect is the increase in the fraction of blue galaxies in the cores of rich, compact, and regular clusters as a function of their redshift (Butcher & Oemler 1978). Over the redshift range of 0 to 0.5, the blue fraction seems to have increased from about 0% to 25% (Butcher & Oemler 1984). Recent observations (Rakos & Schombert 1995) show that this fraction increases to approximately 80% at a redshift of about 1. The nature of the blue galaxies in these clusters appears quite diverse. They could be local spirals, starbursts, AGN types, and some with abnormal spectra (Couch & Sharples 1987). Both ground-based and *Hubble Space Telescope* imaging have further revealed the morphology of the blue galaxies in clusters (Lavery, Pierce, & McClure 1992; Lavery & Henry 1994; Dressler et al. 1994a; Couch et al. 1994; Wirth, Koo, & Kron 1994). Most of the blue galaxies responsible for the B-O effect appear to be late types. Some of them are involved in interactions and mergers. Some appear to be undergoing active star formation or appear to have recently completed star formation.

The B-O effect appears to indicate evolution in cluster galaxies over approximately half the age of the universe. The reasons for this are not entirely clear, although several scenarios exist (Dressler et al. 1994a, 1994b; Aragón-Salamanca et al. 1993; Ostriker & Peebles 1973). It is also unclear if the B-O effect can be explained as an evolutionary effect alone or if other factors, such as the dynamical state of the cluster and the cluster environment, also play a significant role. For example, the cluster Cl 0016+16, at a higher redshift ($z = 0.55$), has a very low fraction (0.02) of blue galaxies in its core, while the cluster Cl 0024+1654 ($z = 0.39$) has a very high fraction (0.16) of blue galaxies (Wirth et al. 1994; Dressler et al. 1985).

An aspect of blue galaxies in clusters that has not yet been explored in detail is their radio continuum property. It is well known that the local sample of galaxies emits a significant amount of nonthermal radio emission. The spectral luminosity at 20 cm of the local spirals is in the range of 10^{18} to $10^{24} \text{ W Hz}^{-1}$. The spectral luminosity of starbursts is in the range 10^{21} to $10^{24} \text{ W Hz}^{-1}$. The early types have a wide range of spectral luminosities, from 10^{20} to $10^{25} \text{ W Hz}^{-1}$. However, at spectral luminosities above $10^{23} \text{ W Hz}^{-1}$, the radio emission from most of the local sample of galaxies is due to an active galactic nucleus (AGN) in them. There is a well-known tight correlation between the spectral luminosity at 20 cm and the far-infrared luminosity of the local sample of spirals (Condon 1992). The far-infrared luminosity of the local sample of spirals ranges from 10^8 to $10^{11} L_{\odot}$. A scenario that explains this tight correlation invokes massive stars to be responsible for both the non-thermal radio emission and the far-infrared luminosity. The nonthermal radio emission from the local spirals is due to the relativistic electrons radiating in the magnetic fields of these galaxies. The relativistic electrons are accelerated by supernova remnants before undergoing diffusion in the galaxy. The supernova remnants are a result of the explosion of massive stars and subsequent evolution. The massive stars are born in molecular clouds and heat the surrounding gas and dust. The heated gas and dust radiate most of their energy in the infrared. Hence one can expect a tight correlation between radio luminosity and far-infrared luminosity in this scenario. If the blue galaxies in clusters responsible for the B-O effect are like the local spirals, then we can expect a similar (to the local) amount of radio continuum emission from them. We can even expect enhanced radio emission from the blue galaxies if they are starbursts, as some of them appear to be. While one can expect the blue

luminosity of a galaxy to be an indicator of its star formation rate, it has been argued that this is not very accurate because of extinction of massive stars in giant molecular clouds and because of a wide range of spectral types that contribute to the blue luminosity of a galaxy (Sage & Solomon 1989). Hence it will be interesting to test the starburst scenario for the blue galaxies from the alternative point of view of their radio continuum emission.

It is also interesting to explore the radio continuum properties of cluster galaxies, whether blue or otherwise, from other points of view. Galaxies in clusters can be subjected to ram-pressure-induced star formation. These stars become supernovae subsequently, leading to the acceleration of cosmic rays and consequent radio emission from these galaxies. The dense cluster gas can confine the relativistic plasma from an AGN in early-type galaxies to produce a brighter radio source. Since the X-ray emission from the intracluster medium essentially traces its density, it is interesting to compare the positions and luminosities of cluster galaxies with the X-ray surface brightness distribution of the cluster. Interactions between galaxies and mergers of galaxies can be expected to be more common in clusters than in the field. Such interactions and mergers can also lead to enhanced star formation or fueling of the AGNs in the centers of these galaxies, leading to enhanced radio emission. Sensitive radio continuum images of clusters can be effectively used in understanding many of these phenomena. Ledlow & Owen (1996) find no differences in the probability of radio emission as a function of environment for spectral luminosities at 20 cm greater than 10^{23} W Hz⁻¹, although below that luminosity the situation could change, as suggested by Sijbring (1993).

In this paper we discuss the results of radio continuum imaging of two clusters, Abell 2125 and Abell 2645, which are similar in their redshifts ($z \sim 0.25$) and richness classes (Abell class 4) but are different in their blue galaxy fractions. A preliminary analysis of these two clusters has already been published (Dwarakanath & Owen 1996). Two other B-O clusters, Abell 370 and Cl 0024+1654, which have also been imaged in the radio continuum in the present observations, will be discussed in a forthcoming publication.

2. OBSERVATIONS

2.1. Radio

A summary of the relevant cluster and observational parameters are given in Table 1. Further details of the clusters can be found elsewhere (Butcher, Oemler, & Wells

1983, hereafter BOW; Butcher & Oemler 1984; Struble & Rood 1991). The criteria for the choice of clusters and the details of radio observations are discussed in Dwarakanath & Owen (1996). A brief summary will be given here. The clusters were observed using the Very Large Array (VLA) in the 20 cm band. All the observations were carried out in the multichannel continuum mode. There were seven channels of 3.125 MHz width for each of four bands (two polarizations \times two bands). The observations were analyzed using the Astronomical Image Processing System developed by the National Radio Astronomy Observatory. For each cluster, the entire primary beam of the VLA dish ($\sim 60'$ at 20 cm) was imaged. The rms values of the noise in the images and the sizes of the synthesized beams are given in Table 1.

2.2. Optical

The optical observations of Abell 2125 and Abell 2645 are described in detail by Owen et al. (1999). We will summarize only the relevant details here. In 1995 August, Owen et al. imaged Abell 2125 and Abell 2645 with the KPNO 0.9 m telescope in *B* and Cousins *R*. The images cover $23' \times 23'$ centered on the clusters, with a 5σ detection limit of $m_R \sim 24.7$. These images were used to make optical identifications of the radio sources detected in the current observations. The accuracy of position measurements on the optical images is $\sigma_{\text{opt}} \sim 0''.2$ (1σ). In the radio images the positional accuracy of a source is $\sigma_{\text{rad}} \sim 0.5\theta_{\text{syn}}/(S/N)$, where θ_{syn} is the FWHM of the synthesized beam (see Table 1) and S/N is the signal-to-noise ratio of the source. The total error (σ) in the agreement between the optical and radio positions is expected to be the sum in quadrature of σ_{opt} and σ_{rad} . The criterion used for optical identification was the agreement between radio and optical positions to within 3σ . The 3σ numbers vary depending on the resolution of the radio images (Table 1). The cluster Abell 2125 was imaged in both the C and A configurations of the VLA. Positions of most, though not all, sources were measured on both these images. The cluster Abell 2645 was imaged in the B configuration of the VLA. For a source with an S/N of 5, the 3σ values adopted were $0''.9$, $1''.5$, and $4''.2$ for the radio images from the A, B, and C configurations, respectively. The results of such an identification process are given in Tables 2 and 3. This criterion of optical identification is adequate in most cases. For a few extended sources, the images from the higher resolution observations were examined to verify the identification process.

TABLE 1
RELEVANT CLUSTER AND OBSERVATIONAL PARAMETERS

CLUSTER	REDSHIFT	N_{30}	f_B	APPROXIMATE FIELD CENTER		VLA CONFIGURATION	SYNTHESIZED BEAM (arcsec)	P.A. (deg)	RMS ($\mu\text{Jy beam}^{-1}$)
				R.A.	Decl.				
Abell 2125	0.2460	62	0.19	15 41.0	+66 18.5	C	13.7×11.5	-7.4	25
				15 41.2	+66 16	A	1.83×1.73	-48.4	~ 30
Abell 2645	0.2500	35	0.03	23 41.6	-09 01.4	B	5.33×4.15	+2.2	27
Abell 370	0.373	107	0.21	02 36.5	-01 34.9	B	5.22×4.25	+23.1	12
Cl 0024+1654...	0.391	87	0.16	00 26.6	+17 10.6	B	4.53×4.32	+23.8	10

NOTES.—Units of right ascension are hours and minutes, and units of declination are degrees and arcminutes (J2000.0). N_{30} is a measure of cluster richness. It indicates 30% of the total number of cluster members brighter than $M_c = -20$. The fraction of blue galaxies in a cluster (f_B) is the fraction of the total net cluster population with rest-frame *B-V* colors at least 0.2 mag bluer than those of the early-type galaxies (Butcher & Oemler 1984). The VLA configurations A, B, and C have maximum baselines of approximately 35, 11, and 3 km, respectively.

TABLE 2
ABELL 2125: OPTICAL IDENTIFICATIONS

SOURCE	RADIO POSITION		SEPARATION (arcsec)	EXTENT (arcsec)	P.A. (deg)	MEMBER?	STAR FORMATION?	S_{20} (μ Jy)	L_{20} (10^{22} W Hz $^{-1}$)
	R.A.	Decl.							
1	15 39 08.68	66 08 54.2	0.87	18.9 × 5.2	12	Y	N	63174	897
2	15 39 33.20	66 07 44.1	1.0	2.8 × 1.5	49	1231	...
3	15 39 46.17	66 06 25.7	4.1	10.6 × 1.9	90	87206	...
4	15 39 59.40	66 11 27.2	0.64	Y	Y	265	3.7
5	15 39 59.39	66 16 07.9	0.50	9.4 × 2.2	82	Y	N	9284	132
6	15 40 00.05	66 05 52.0	0.50	1.5 × 0.6	33	29560	...
7	15 40 05.42	66 10 13.3	0.52	Y	N	486	6.9
8	15 40 08.67	66 15 36.4	0.2	N	...	114	...
9	15 40 09.31	66 12 17.7	1.7	7 × 7	100	Y	N	431	6.1
10.....	15 40 12.09	66 12 10.6	0.72	Y	N	211	3.0
11.....	15 40 15.88	66 11 10.8	0.92	Y	Y	314	4.5
12.....	15 40 25.94	66 30 30.3	0.38	Y	N	265	3.8
13.....	15 40 30.10	66 12 14.6	0.35	13.3 × 7	5	Y	Y	181	2.6
14.....	15 40 30.36	66 13 04.1	2.3	Y	N	146	2.1
15.....	15 40 30.82	66 12 27.1	0.97	Y	Y	148	2.1
16.....	15 40 33.63	66 08 01.7	0.21	652	...
17.....	15 40 39.86	66 13 10.0	1.1	Y	Y	137	1.9
18.....	15 40 41.05	66 26 55.6	1.9	N	...	1891	...
19.....	15 40 42.50	66 08 54.5	0.4	396	...
20.....	15 40 43.19	66 10 21.1	0.3	214	...
21.....	15 40 48.66	66 18 37.9	3.7	24.3 × 5.4	120	Y	N	15820	224
22.....	15 40 50.90	66 16 31.4	0.9	N	...	93	...
23.....	15 40 51.86	66 06 31.1	0.38	N	...	439	...
24.....	15 40 53.71	66 05 26.5	0.44	Y	Y	196	2.8
25.....	15 40 54.54	66 11 28.2	0.72	211	...
26.....	15 40 54.66	66 17 16.4	0.7	Y	N	299	4.2
27.....	15 40 56.90	66 26 46.5	0.7	Y	N	259	3.7
28.....	15 41 00.71	66 13 53.2	1.6	127	...
29.....	15 41 01.92	66 16 27.2	0.6	Y	N	205	2.9
30.....	15 41 05.16	66 12 34.4	1.6	N	Y	109	1.5
31.....	15 41 07.32	66 21 23.8	0.2	150	...
32.....	15 41 09.74	66 15 45.0	0.5	0.3 × 0.3	22	Y	Y	23205	330
33.....	15 41 10.88	66 13 13.2	1.7	126	...
34.....	15 41 14.38	66 15 57.6	0.8	2.7 × 0.9	11	Y	N	3058	43.4
35.....	15 41 14.40	66 21 40.4	1.3	8.2 × 4.1	121	N	...	435	...
36.....	15 41 14.89	66 16 04.3	0.74	2.1...0.9	125	Y	N	516	7.3
37.....	15 41 15.24	66 15 57.5	1.6	Y	N	15502	220
38.....	15 41 28.02	66 13 26.7	3.2	11 × 11	170	N	...	652	...
39.....	15 41 33.88	66 22 55.9	1.2	179	...
40.....	15 41 33.68	66 31 11.4	1.80	Y	N	536	7.6
41.....	15 41 40.92	66 22 38.5	0.82	3.6 × 2.5	105	34412	...
42.....	15 41 43.30	66 15 16.9	0.58	Y	N	165	2.3
43.....	15 41 48.84	66 11 37.6	0.67	1646	...
44.....	15 42 02.87	66 15 53.8	1.5	Y	Y	136	1.9
45.....	15 42 03.85	66 26 32.3	0.63	1.3 × 0.9	133	Y	Y	314	4.5
46.....	15 42 14.54	66 30 03.4	1.0	N	...	352	...
47.....	15 42 24.27	66 19 59.4	1.0	Y	N	196	2.8
48.....	15 42 24.76	66 29 03.7	0.81	N	...	168	...
49.....	15 42 25.16	66 09 17.7	0.73	216	...
50.....	15 42 41.04	66 24 37.5	0.67	N	Y	342	4.9
51.....	15 42 41.33	66 24 34.6	1.1	N	Y	317	4.5
52.....	15 43 01.14	66 15 17.8	1.0	484	...
53.....	15 43 07.81	66 13 43.9	0.0	200	...
54.....	15 43 44.96	66 30 01.2	0.81	1.5 × 0.4	67	Y	Y	547	7.8

NOTES.—Units of right ascension are hours, minutes, and seconds, and units of declination are degrees, arcminutes, and arcseconds (J2000.0). Separation is the radial distance between the optical and radio positions. The extent is as measured in the radio images. The luminosities are in the observer's rest frame and are estimated using $z = 0.2460$, $H_0 = 75 \text{ km s}^{-1} \text{ Mpc}^{-1}$, and $q_0 = 0.1$.

TABLE 3
ABELL 2645: OPTICAL IDENTIFICATIONS

SOURCE	RADIO POSITION		SEPARATION (arcsec)	EXTENT (arcsec)	P.A. (deg)	MEMBER?	STAR FORMATION?	S_{20} (μ Jy)	L_{20} (10^{22} W Hz $^{-1}$)
	R.A.	Decl.							
1	23 40 27.90	-9 09 43.7	2.47	N	Y	214	...
2	23 40 39.56	-8 51 37.1	1.56	129	...
3	23 40 43.18	-8 53 56.6	1.47	148	...
4	23 40 45.51	-9 01 55.0	1.1	266	...
5	23 40 49.35	-8 57 03.7	1.25	170	...
6	23 40 53.08	-9 03 15.3	0.9	N	...	316	...
7	23 40 52.22	-8 58 30.1	0.9	N	Y	267	...
8	23 40 57.04	-9 01 53.7	0.75	N	N	153	...
9	23 41 07.73	-8 55 45.8	1.3	123	...
10	23 41 10.19	-8 57 11.9	0.18	Y	N	674	9.9
11	23 41 11.54	-9 00 04.0	0.78	N	N	286	...
12	23 41 11.50	-8 44 46.3	1.66	4×1.7	21	Y	N	7020	103
13	23 41 11.57	-9 02 02.2	1.21	Y	N	2607	38.2
14	23 41 13.04	-9 02 12.4	0.72	1412	...
15	23 41 13.99	-9 07 47.8	0.58	N	N	483	...
16	23 41 15.28	-9 05 17.0	0.00	1257	...
17	23 41 16.20	-8 55 09.6	1.05	112	...
18	23 41 17.11	-9 02 17.0	0.83	105	...
19	23 41 20.76	-8 55 42.1	0.20	N	Y	257	...
20	23 41 21.97	-9 02 13.5	0.52	N	Y	255	...
21	23 41 26.03	-9 04 49.3	0.80	338	...
22	23 41 37.29	-8 51 54.2	1.08	223	...
23	23 41 37.54	-9 11 00.0	1.01	153	...
24	23 41 37.86	-9 03 11.7	0.62	129	...
25	23 41 39.45	-9 02 11.4	0.90	N	N	174	...
26	23 41 39.66	-8 48 36.0	1.00	577	...
27	23 41 40.68	-8 43 10.8	2.62	N	Y	204	...
28	23 41 42.36	-9 14 31.7	0.85	N	N	285	...
29	23 41 44.1	-9 08 00.2	0.15	578	...
30	23 41 57.99	-8 55 16.2	0.25	N	N	5437	...
31	23 41 59.74	-9 02 05.8	0.90	129	...
32	23 41 59.76	-9 03 48.5	0.42	N	N	312	...
33	23 42 03.31	-9 03 00.4	0.50	305	...
34	23 42 3.04	-9 04 25.5	1.10	N	N	209	...
35	23 42 03.36	-8 51 27.2	1.04	3.2×0.4	34	Y	N	1255	18.4
36	23 42 04.98	-8 58 31.5	0.91	N	N	194	...

NOTES.—Units of right ascension are hours, minutes, and seconds, and units of declination are degrees, arcminutes, and arcseconds (J2000.0). Separation is the radial distance between the optical and radio positions. The extent is as measured in the radio images. The luminosities are in the observer's rest frame and are estimated using $z = 0.2500$, $H_0 = 75 \text{ km s}^{-1} \text{ Mpc}^{-1}$, and $q_0 = 0.1$.

Spectroscopy was obtained for the optical identifications using a long slit on the KPNO 4 m telescope with the Ritchey-Chrétien spectrograph (Owen et al. 1999). Inside of a circle 2.5 Mpc in diameter ($\sim 12'$ for $z = 0.25$, $q_0 = 0.1$, and $H_0 = 75 \text{ km s}^{-1} \text{ Mpc}^{-1}$) in projection at the cluster redshift, redshifts for all the optical identifications brighter than $m_R = 19.5$ were obtained (Owen et al. 1999).

3. RESULTS

The results of optical identifications in the fields toward Abell 2125 and Abell 2645 are summarized in Tables 2 and 3, respectively. The sources are arranged in increasing order of right ascension. The flux densities quoted in the tables are integrated values for extended sources and peak values for unresolved sources. The last column contains spectral luminosities for cluster members. In Abell 2125 (Table 2) there are 54 optical identifications. The mean separation between the centroids of radio and optical positions of these 54 sources is approximately $1''.0$. Their membership in the cluster is indicated under the column headed "Member?" There are some optical identifications that do not have spectroscopy, and hence their membership is unknown.

There are 27 cluster members, with a mean redshift of 0.2460 ± 0.0007 and a dispersion of 891 km s^{-1} (Owen et al. 1999).

The cluster galaxies have been divided into two categories based on the presence or absence of star formation in them. Current star formation activity in galaxies is accompanied by the presence of emission lines, small D_{4000} break, and bluer colors (small $B - R$ values). Such galaxies will be referred to as star-forming galaxies (SFGs) and are indicated in Tables 2 and 3 with a "Y" in the column headed "Star Formation?" Galaxies devoid of such evidence will be referred to as non-star-forming galaxies (NSFGs) and are indicated in Tables 2 and 3 with an "N" in the same column. There are 10 SFGs and 17 NSFGs in Abell 2125. It is interesting to note that, while the mean velocities of these two classes of galaxies are within 100 km s^{-1} of each other, their velocity dispersions differ by about 400 km s^{-1} . Further classification of these galaxies into old, intermediate, starburst, and AGN systems have been made by Owen et al. (1999).

In the field toward Abell 2645, there are only 36 optical identifications (Table 3). As a fraction of the total number of

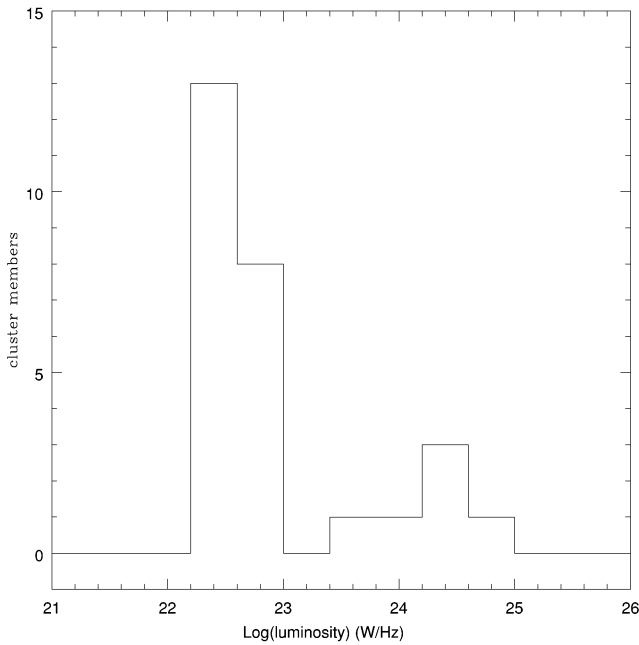


FIG. 1.—Distribution of Abell 2125 cluster members as a function of spectral luminosity at 20 cm. The spectral luminosity at 20 cm is from Table 2. The lower cutoff in the distribution is due to the detection limit of the radio observations. A detection limit of $100 \mu\text{Jy}$ corresponds to 22.15 along the x-axis. The total number of sources in the histogram is 27.

radio sources detected in this field, this number is consistent with that toward Abell 2125. In both directions, about 16% of the radio sources have been identified with their optical counterparts. However, the surprising result is that a very small fraction of these are members of the Abell 2645 cluster. There are four cluster members (marked “Y” in Table 3), with a mean redshift of 0.2500 ± 0.0020 (Owen et

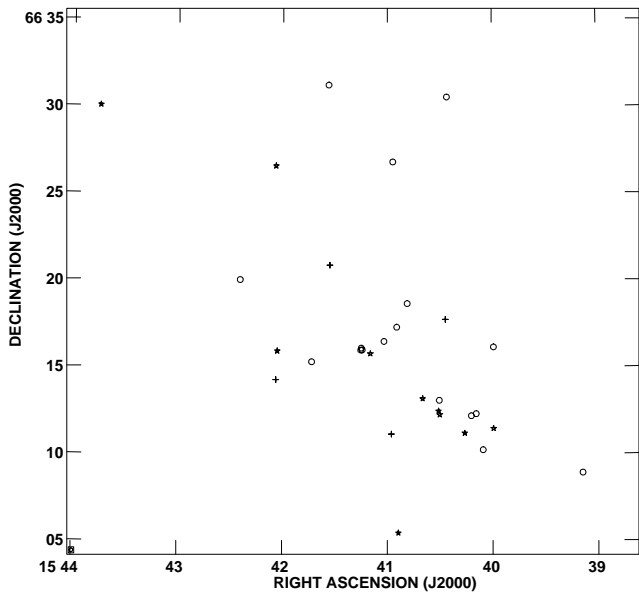


FIG. 2.—Distribution of cluster members projected in the plane of the sky. There are 27 members. The stars represent radio sources that show signs of star formation (SFGs). The circles represent radio sources that do not show signs of star formation (NSFGs). The crosses represent the four corners of the square field observed in the optical by BOW. An angular separation of $5'$ corresponds to a proper length of about 1 Mpc. The synthesized beam is shown at the bottom left corner of the figure.

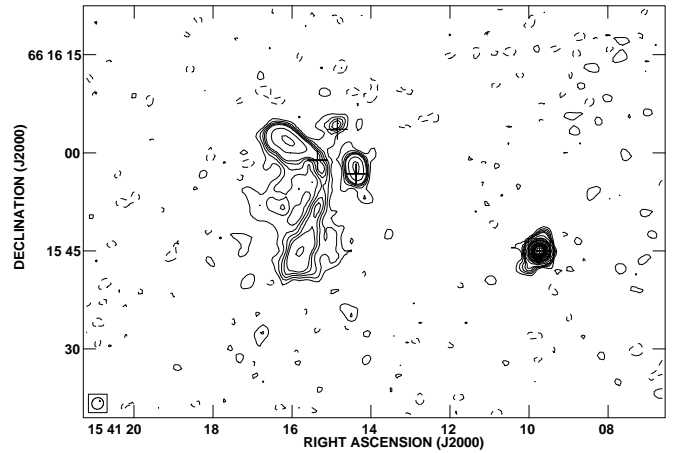


FIG. 3.—Radio images of some cluster members (sources 32, 34, 36, and 37 in Table 2) made with the VLA in its A configuration (maximum baseline ~ 35 km). The crosses mark the positions of optical identifications. The bright source (32 in Table 2) shows signs of star formation although it is an AGN, while the other three sources (34, 36, and 37 in Table 2) do not show any signs of star formation. The contours are in steps of $60 \mu\text{Jy beam}^{-1}$ from -120 to $300 \mu\text{Jy beam}^{-1}$ (excluding the contour at $0 \mu\text{Jy beam}^{-1}$), in steps of $0.6 \text{ mJy beam}^{-1}$ from 0.6 to 3 mJy beam^{-1} , in steps of $1.5 \text{ mJy beam}^{-1}$ from 4.5 to 15 mJy beam^{-1} , and in steps of 3 mJy beam^{-1} from 18 mJy beam^{-1} to 30 mJy beam^{-1} . The synthesized beam is at the bottom left corner.

al. 1999). Toward the direction of Abell 2125 about half of the optical identifications are cluster members, while toward Abell 2645 only approximately 10% of the optical identifications are cluster members.

The distribution of Abell 2125 cluster members as a function of spectral luminosity at 20 cm is shown in Figure 1. The spectral luminosities were estimated based on the values of $z = 0.2460$, $H_0 = 75 \text{ km s}^{-1} \text{ Mpc}^{-1}$, and $q_0 = 0.1$. The spectral luminosity (in the rest frame of the observer) at

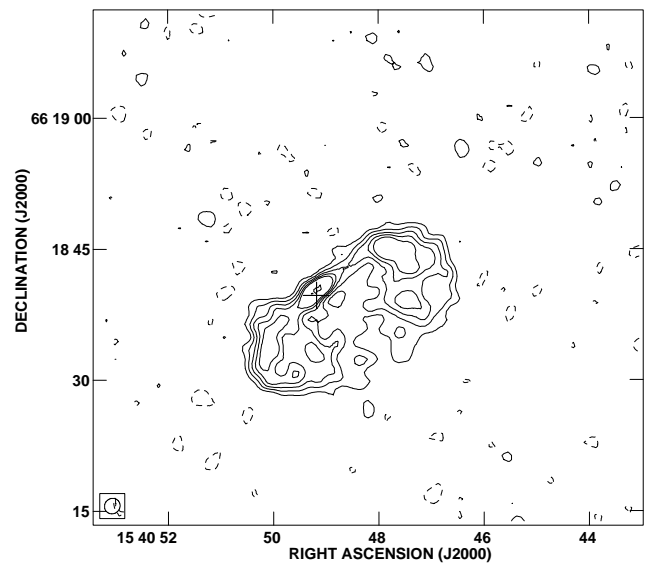


FIG. 4.—Radio image of another cluster member (source 21 in Table 2) made with the VLA in its A configuration. This source shows no signs of star formation. The cross marks the position of the optical identification. The radio morphology resembles that of FR I sources. The cluster center is toward the bottom left corner. Contours are the same as in Fig. 3.

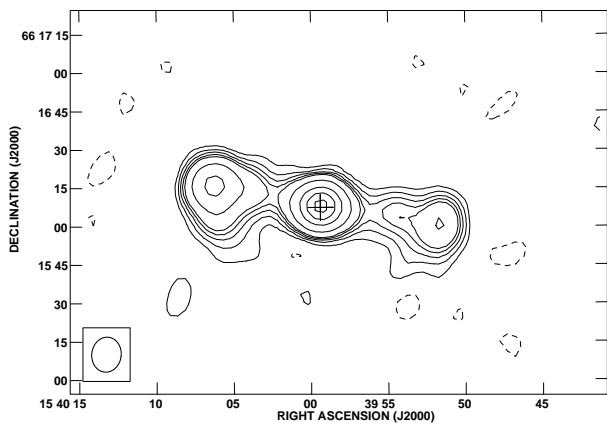


FIG. 5.—Radio image of another cluster member (source 5 in Table 2) made with the VLA in its C configuration. This source shows no signs of star formation. The cross marks the position of the optical identification. Contours are the same as Fig. 3.

20 cm, L_{20} , is related to the continuum flux density at 20 cm, S_{20} , as $L_{20} = 1.42 \times 10^{20} S_{20} \text{ W Hz}^{-1}$, where S_{20} is in μJy . There are 27 sources in Figure 1. The lower cutoff corresponds to the detection limit (5σ) of the radio observations at approximately $100 \mu\text{Jy beam}^{-1}$. A bimodal distribution is apparent with the two classes centered around spectral luminosities of 4×10^{22} and $2.5 \times 10^{24} \text{ W Hz}^{-1}$.

The distribution of Abell 2125 cluster members as projected on the sky is shown in Figure 2. The distribution is elongated, with a northeast-to-southwest extent of about 5 Mpc. There appears to be a clustering of members in the southwest position just outside the box defined by the four

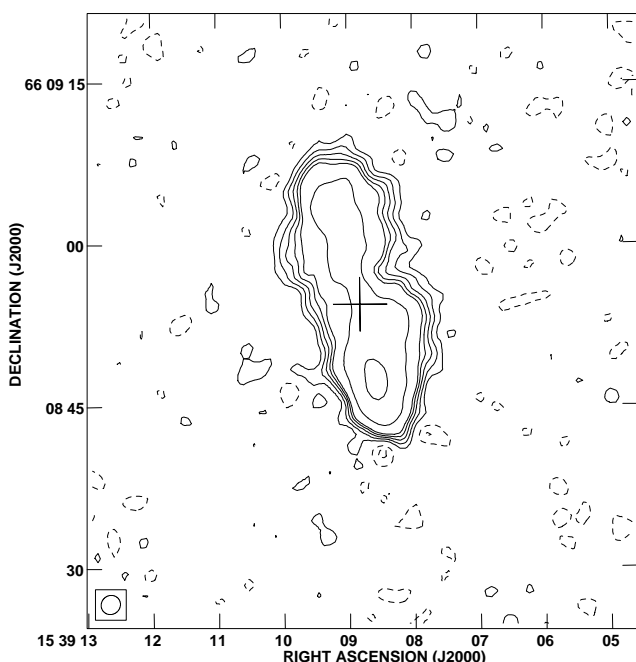


FIG. 6.—Radio image of cluster member (source 1 in Table 2) made with the VLA in its A configuration. The cross marks the position of the optical identification. The contours are in steps of $100 \mu\text{Jy beam}^{-1}$ from -200 to $500 \mu\text{Jy beam}^{-1}$ (excluding the contour at $0 \mu\text{Jy beam}^{-1}$) and at 1 and 2 mJy beam^{-1} .

crosses. There are four NSFGs and five SFGs in this group. Their mean velocity is essentially identical to that of the cluster. The velocity dispersion of this group is about 100 km s^{-1} less than that of the cluster. Some of the more interesting radio images of Abell 2125 cluster members are shown Figures 3, 4, 5, and 6.

4. DISCUSSION

4.1. Blue Galaxies in Abell 2125

The central 55 arcmin^2 of the Abell 2125 cluster were studied by BOW as part of their broadband photometric study of nearby and distant ($z = 0.5$) clusters. The region covered by them in Abell 2125 is enclosed by the four crosses in Figure 2 (see Dwarakanath & Owen 1996 for a radio continuum image of this region). Within this region there are 17 galaxies (to a red magnitude limit of 22 mag) whose colors as measured by their values of $J-F$ ($J-F < 1.6$) are considered “blue” by BOW. Of these, only three galaxies have radio sources in the present observations near enough ($< 5''$) to be considered as possible counterparts. Based on recent spectroscopy (Owen et al. 1999), two of these are not members of the Abell 2125 cluster. The third source is a cluster member. This is source 32 in Table 2 and source 33 in BOW. A radio image of this source made with the VLA in its A configuration is shown in Figure 3. Thus, to the detection limit (5σ) of $1.42 \times 10^{22} \text{ W Hz}^{-1}$, only one out of the 17 blue galaxies was detected in radio.

One of the motivations for the present study was to detect radio emission from the blue galaxies in the central regions of the Abell 2125 cluster that are responsible for the B-O effect. Many nearby spiral galaxies are known to be radio sources. Their radio emission is believed to be due to current star formation and subsequent supernova activity. The radio emission can thus be related to the current supernova rate. There is an observed Galactic relation between the nonthermal radio luminosity L_N (in units of $10^{22} \text{ W Hz}^{-1}$) and the supernova rate (yr^{-1}) v_{sn} , which implies $L_N \sim 13v^{-\alpha}v_{\text{sn}}$, where v is in GHz (Condon & Yin 1990). If this relation is applicable to the blue galaxies in Abell 2125, then the absence of radio emission to the detection limit mentioned above implies that the supernova rate in the blue galaxies is less than 0.1 yr^{-1} . As a comparison, the supernova rate in our Galaxy is approximately 0.041 yr^{-1} (Tammann 1982) and that in M82 is about 0.1 yr^{-1} (Condon 1992). It appears from this point of view that the current star formation rate in the blue galaxies is less than that in M82 and might even be comparable to our own Galaxy. Of course, these arguments do not rule out the possibility of the blue galaxies having had an intense starburst phase at an earlier ($> 10^8 \text{ yr}$) epoch. This time limit corresponds to the half-life of relativistic electrons against synchrotron losses radiating in the 20 cm band for an assumed magnetic field of $5 \mu\text{G}$. Interestingly, Abraham et al. (1996) come to a similar conclusion about the blue galaxies in Abell 2390 insofar as their star formation rates are concerned.

As was mentioned earlier, there is only one galaxy (source 32 in Table 2) out of the 17 blue galaxies studied by BOW that was detected in radio and has a high radio luminosity of $3.3 \times 10^{24} \text{ W Hz}^{-1}$. Although there is some evidence of star formation in this galaxy in the form of smaller D_{4000} break, its spectrum and radio luminosity indicate this to be

an active galactic nucleus (Owen et al. 1999). Most of its radio emission is due to the AGN activity.

4.2. *Abell 2125 Cluster Members*

The distribution of cluster members as a function of radio luminosity at 20 cm appears bimodal (Fig. 1). There is one class of galaxies around $\log(\text{luminosity})$ of 22.6 and another around 24.5. About half the galaxies in the low-luminosity class are SFGs, while only about 15% of the galaxies in the high-luminosity class are SFGs. The rest are NSFSGs. The fraction of SFGs is significantly smaller in the high-luminosity class of galaxies. One possible reason for this is an upper limit to the nonthermal radio luminosity of SFGs due to an upper limit to their supernova rate. If the relation between L_N and v_{sn} mentioned in the previous section is applicable to the galaxies in Abell 2125, then the low radio luminosity galaxies require a supernova (SN) rate of about 0.3 yr^{-1} . This is close to the maximum SN rate observed in nearby external galaxies (Tammann 1982). Hence, it is quite reasonable to expect a significant fraction of the low radio luminosity galaxies in Abell 2125 to be SFGs. The high radio luminosity galaxies in Abell 2125, on the other hand, would require 2 orders of magnitude higher SN rate in SFGs if their radio emission were due to star formation related processes. Such a high SN rate is possible only if a galaxy is in its intense starburst phase. Hence, it is not surprising to find a small fraction of SFGs in the high radio luminosity cluster members. Most of the radio emission of these high radio luminosity galaxies must be due to their AGN activity. In Figures 3, 4, 5, and 6 the radio morphologies of some of the high radio luminosity galaxies in Abell 2125 are shown.

The projected distribution of cluster members (Fig. 2) is elongated along the northeast-to-southwest direction. This is similar to the observed surface brightness distribution in X-rays, although there is no detailed correlation between the position and the type of galaxies with the X-ray surface brightness. A scenario that attempts to explain the X-ray morphology is that Abell 2125 is a rich assembly of galaxies and is still at its early evolutionary stage to become a rich X-ray-emitting cluster (Wang, Connolly, & Brunner 1997). This implies that Abell 2125 is not yet completely virialized. There are perhaps some indications of this in the observations reported here. The cluster members (Fig. 2) can be divided into three classes—the SFGs, the NSFSGs, and the Southwest group. The mean velocities of these three classes are within 40 km s^{-1} of each other, while their velocity dispersions differ by about 400 km s^{-1} . Differences in velocity dispersions for early- and late-type galaxies in clusters have been reported earlier (Biviano et al. 1997 and references therein). It is quite likely that the differences in the velocity dispersions of the three classes in Abell 2125 are due to their different kinematics. However, since the number of cluster members in each class is small, the errors on the velocity dispersions are quite large. The existing data are inadequate to comment on the significance of the different velocity dispersions of the three classes.

There appears to be a radial dependence of the ratio of SFGs to NSFSGs. From Figure 2 it is clear that while this ratio is very small ($\sim 15\%$) in the central regions of the cluster (the area enclosed by the crosses) the ratio increases to approximately 50% in the southwest group. This is reminiscent of the Coma Cluster, in which the southwest group contains a larger fraction of galaxies undergoing recent star

formation or nuclear activity. In contrast, very few such galaxies are found in the central regions of the Coma Cluster (Caldwell et al. 1993). The southwest group in Abell 2125 probably represents a subcluster of similar nature.

4.3. *The Abell 2645 Cluster*

Although Abell 2125 and 2645 have similar redshifts and richnesses, the number of radio sources in these two clusters differs by a factor of 10. Since both the clusters have been observed to the same luminosity limit in radio and optical, this difference cannot be due to missing the weaker cluster members in Abell 2645. All the four cluster members in Abell 2645 are NSFSGs with radio luminosities at 20 cm over $10^{23} \text{ W Hz}^{-1}$. It is as though the entire low-luminosity class detected in Abell 2125 (Fig. 1) is missing in Abell 2645. One possible reason for this difference could be that these two clusters are in different stages of their evolution. The cluster Abell 2125 is not yet fully virialized and is still undergoing merging of the subclusters. As a consequence, most of the cluster members retain their gas content, which is responsible for radio emission in SFGs (through star formation) and in NSFSGs (through fueling the AGN). If Abell 2645 is already virialized, most of the cluster members would have lost their gas to the intracluster medium, resulting in reduced gas supply and radio emission.

5. SUMMARY

The Abell clusters 2125 and 2645 were imaged in radio to the same luminosity limit at 20 cm of $1.4 \times 10^{22} \text{ W Hz}^{-1}$ using the Very Large Array. These two clusters are similar in richness (class 4) and redshift ($z \sim 0.25$). However, the blue galaxy fractions of Abell 2125 and Abell 2645 are 0.19 and 0.03, respectively (Butcher & Oemler 1984). Based on photometry and spectroscopy of these clusters to the same limiting magnitude by Owen et al. (1999), the cluster memberships and the nature of the radio sources were established. There are 27 confirmed members in Abell 2125 but only four in Abell 2645. The projected distribution of Abell 2125 members is elongated with a northeast-to-southwest extent of about 5 Mpc. About half the members show signs of star formation, with the largest concentration of star-forming galaxies in the southwest clump. There is a bimodal distribution of Abell 2125 members in radio luminosity, with the majority below a spectral luminosity at 20 cm of $10^{23} \text{ W Hz}^{-1}$. About half of these galaxies show signs of star formation. The high radio luminosity members appear to be AGNs. Only one out of the 17 blue galaxies responsible for the B-O effect in Abell 2125 was detected in radio. The current supernova rate in the blue galaxies from which no radio emission was detected is less than 0.1 yr^{-1} . The entire low radio luminosity ($< 10^{23} \text{ W Hz}^{-1}$) class of galaxies that was detected in Abell 2125 is absent in Abell 2645. The different dynamical states of the two clusters might be responsible for the differences in the radio source populations observed in these two clusters, as well as the Butcher-Oemler effect.

We thank the referee for useful comments on an earlier version of the manuscript. The National Radio Astronomy Observatory is a facility of the National Science Foundation operated under cooperative agreement by Associated Universities, Inc.

REFERENCES

- Abraham, R. G., et al. 1996, *ApJ*, 471, 694
Aragón-Salamanca, A., Ellis, R. S., Couch, W. J., & Carter, D. 1993, *MNRAS*, 262, 764
Biviano, A., Katgert, P., Mazure, A., Moles, M., den Hartog, R., Perea, J., & Focardi, P. 1997, *A&A*, 321, 84
Butcher, H. R., & Oemler, A., Jr. 1978, *ApJ*, 219, 18
———. 1984, *ApJ*, 285, 426
Butcher, H. R., Oemler, A., Jr., & Wells, D. C. 1983, *ApJS*, 52, 183
Caldwell, N., Rose, J. A., Sharples, R. M., Ellis, R. S., & Bower, R. G. 1993, *AJ*, 106, 473
Condon, J. J. 1992, *ARA&A*, 30, 575
Condon, J. J., & Yin, Q. F. 1990, *ApJ*, 357, 97
Couch, W. J., Ellis, R. S., Sharples, R. M., & Smail, I. 1994, *ApJ*, 430, 121
Couch, W. J., & Sharples, R. M. 1987, *MNRAS*, 229, 423
Dressler, A., Gunn, J. E., & Schneider, D. P. 1985, *ApJ*, 294, 70
Dressler, A., Oemler, A., Jr., Butcher, H. R., & Gunn, J. E. 1994a, *ApJ*, 430, 107
Dressler, A., Oemler, A., Jr., Sparks, W. B., & Lucas, R. A. 1994b, *ApJ*, 435, L23
Dwarakanath, K. S., & Owen, F. N. 1996, in *Cold Gas at High Redshift*, ed. M. N. Bremer, P. P. van der Werf, H. J. A. Röttgering, & C. L. Carilli (Dordrecht: Kluwer), 183
Lavery, R. J., & Henry, J. P. 1994, *ApJ*, 426, 524
Lavery, R. J., Pierce, M. J., & McClure, R. D. 1992, *AJ*, 104, 2067
Ledlow, M. J., & Owen, F. N. 1996, *AJ*, 112, 9
Ostriker, J. P., & Peebles, P. J. E. 1973, *ApJ*, 186, 467
Owen, F. N., Ledlow, M. J., Keel, W. C., & Morrison, G. E. 1999, *AJ*, 118, 633
Rakos, K. D., & Schombert, J. M. 1995, *ApJ*, 439, 47
Sage, L. J., & Solomon, P. M. 1989, *ApJ*, 342, L15
Sijbring, D. 1993, Ph.D. thesis, Univ. Groningen
Struble, M. F., & Rood, H. J. 1991, *ApJS*, 77, 363
Tammann, G. A. 1982, in *Supernovae: A Survey of Current Research*, ed. M. J. Rees & R. J. Stoneham (Dordrecht: Reidel), 371
Wang, Q. D., Connolly, A. J., & Brunner, R. J. 1997, *ApJ*, 487, L13
Wirth, G. D., Koo, D. C., & Kron, R. G. 1994, *ApJ*, 435, L105